Low-Cost Hydrothermal Synthesis of Porous Carbon Spheres with Tunable Particle Size

JungHwa Hong, Alexandre Magasinski, Gleb Yushin*

School of Materials Science and Engineering, Georgia Institute of Technology, Atlanta, Georgia 30332, USA

*Email: yushin@gatech.edu

Abstract

Spherical porous carbon particles find applications in gas storage, biological and medical sorbents, energy storage devices and other demanding applications. At the same time, the common routes for their synthesis are elaborate and costly. Here we report on our study of a low-cost synthesis of spherical carbons with uniform and tunable diameter. The application of a low-temperature hydrothermal process greatly accelerates the rate of cross-linking within polymer precursors, allowing formation of individual spherical carbon particles upon subsequent polymer carbonization. By reducing the precursor concentration we have demonstrated particle size reduction from 1,250 to 140 nm. The as-produced particles exhibit disordered microstructure with very smooth particle surface and open internal micro-porosity.

Sorption-desorption

1. Introduction

Spherical particles of porous carbons may find widespread applications in various fields, such as electrodes in electrical double layer capacitors and asymmetric electrochemical capacitors,[1] hosts for anode and cathode active materials for high-capacity Li ion batteries,[2] catalyst support,[3] gas storage,[4] water purification,[5] photonic crystals,[6] additives and lubricating materials,[7] blood cleansing,[8] cellular delivery and drug delivery and other medical applications,[9] to name a few. Carbon (nano)particles are nontoxic, biocompatible, and non-immunogetic.[10]

The spherical shape of carbon particles may provide a combination of unique benefits for various applications. For batteries and electrochemical capacitors, for example, spherical powder shape leads to higher rate electrode performance. This is because when electrodes composed of spherical particles are densified (calendared) to maximize their volumetric performance and reduce electrical resistance, they still allow for a rapid electrolyte transport through interstitials between the packed spheres. Spherical particles are also easier to process into uniform smooth electrode films, which shall reduce the problems of local anode-cathode misbalance, occasionally faced by electrodes composed of larger irregularly particles and known to induce full cell degradation. Similar benefits (combination of high volumetric performance and high rate capability) are also valid for carbon use in gas storage, gas separation and purification of various liquids. For medical and biological applications, smooth particle surfaces are important to avoid contamination of biological media by small carbon debris and to avoid penetration of cells by sharp features of the randomly shaped particles. For academic studies, regularly sized spherical particles allow one to clearly observe morphological changes or the formation of undesirable defects or precipitates on the particles.

A common way to synthesize carbon spheres is the so-called nanocasting or templating strategy, which employs sacrificial inorganic templates (such as silica) for filling with a carbon precursor for the subsequent polymerization, carbonization and chemical leaching of the silica template[11]. This method suffers from a very high cost and is believed not to be industrially unfeasible and commercially viable for the majority of applications.[12] Another rather common method involves using soft templates.[13, 14]. However, complete and delicate removal of organic templates can be challenging, which leads to a limited control of the shape of the product [13] The use of alternative synthesis methods, such as emulsion-assisted synthesis in water-alcohols' mixtures,[15] has been very limited. A decade ago, significant research has been focused on the formation of resorcinol (R) – formaldehyde (F) sol-gels and the extensive review on such a subject has been published.[16] This method involves mixing F and R in the presence of a catalyst at elevated temperatures to produce a cross-linked polymer gel. The produced gel is commonly dried either supercritically to produce an organic aerogel or subcritically to produce a xerogel. The material could be further carbonized to produce a highly porous carbon network.[16] The studies demonstrated very uniform distribution of the primary particle sizes and different synthesis conditions yielded primary particles of various sizes. Furthermore, under certain conditions individual or only weekly bonded carbon particles have been produced.[16]

To follow up on these previous studies and to develop spherical carbon materials for energy storage applications we were interested to further explore the opportunities offered by R-F

chemistry. We were specifically interested to be able to show simple means to tune the particle size distribution, since the time of ion diffusion within individual particles (and thus power performance of energy storage devices) are strongly size dependent.[18]

Hydrothermal carbonization (HTC) process offers a low-cost, low-temperature route for transformation of virtually any carbonaceous organic materials into porous carbons decorated with numerous polar oxygenated functionalities. [19] In our previous studies we demonstrated that uniformly distributed functional groups allow one to uniformly enlarge micropores of HTC carbons by activation and produce uniform, highly porous carbons with outstanding performance in supercapacitor electrodes.[20] In this manuscript we present a systematic study of the bottom-up synthesis of R-F derived carbon nanospheres with controlled particle size using an HTC apparatus. This procedure is simple and is cost effective as well as being environmentally friendly, using only resorcinol, formaldehyde and small amount of ammonia as precursors.

2. Experimental

2.1 Synthesis

2.1.1 Chemicals

Formaldehyde (F) (CH_2O) 37 wt. % aqueous solution stabilized with 8% methanol was purchased from Alfa Aesar (USA). Resorcinol (R) (1,3-dehydroxybenzene, $C_6H_4(OH)_2$) 99 % was also purchased from Alfa Aesar (USA). The amount of F & R was in each experiment according to the Table 1. The amount of ammonium hydroxide (NH_3OH) catalyst (0.2 ml of 30 % solution in H_2O, Alfa Aesar, USA) and the amount of distilled H_2O (40 ml) was the same for each experiment.

2.1.2 Synthesis

The synthesis of the carbon spheres can be devided into three steps: (i) polymerization of the precursors (R & F) to form spherical particles (often called “globules”), (ii) condensation of the material during the hydro-thermal treatment, and (iii) carbonization during annealing under inert environment. Distilled H_2O and NH_3OH were first mixed for 1h at 30 °C in a 50 ml flat bottom round flask with a magnetic stirrer rotating in 600 rpm. The designated amount of R and F was added to the system and mixed overnight (12 h). Subsequently, the solution was put through hydro-thermal treatment using the 4565 Parr (IL, USA) hydro thermal mini-reactor apparatus at 100 °C for 12 h. Thus produced solid product was separated from the solution using the centrifuge operating at 6200 rpm (4 min.), washed with distilled H_2O and separated again. The procedure was repeated 3 times to warrant high purity. Then the product was air-dried in a convection oven at 80 °C and carbonized in a tube furnace under Ar flow at 350 °C for 2h and at 600 °C for 4 h. The heating rate was 1C°/min.

2.2 Characterization

Scanning electron microscopy (ZEISS LEO 1530, Germany) was conducted at a working distance of 5-10 mm and accelerating voltage of 5-10 kV to characterize the size and shape of the produced powder. Transmission electron microscopy (TEM) measurements were conducted on JEOL 100CX II transmission electron microscope (JEOL, Japan) operated at 100 kV to reveal the particles’ uniformity. The nitrogen (N_2) adsorption-desorption isotherms were collected at 77K on

a Micromeritics Tristar 3000 system (GA, USA) to measure the pore size distribution. Prior to the measurements, all samples were out-gassed at 300 °C for at least 6h. The Brunauer-Emmett-Teller (BET) specific surface areas (SSA) were calculated using the absorption data. Pore size distributions were derived from the adsorption branch using a non-linear (NL) density functional theory (DFT) method. The total pore volumes were estimated from the amounts adsorbed at the relative pressure (P/Po) of 0.99. The X-ray diffraction (XRD) (PANalytical X'Pert PRO Alpha-1, USA) measurements utilized 1.8 kW Ceramic Copper tube as an X-ray source (settings 45kV, 40mA) and PW3050/60 goniometer for varying the 2θ angle.

3. Results and Discussion

The resorcinol-formaldehyde (R-F) polymer is classified as a phenolic resin. The R reacts with F to form hydroxymethylated resorcinol (XMR) with hydroxymethyl (-CH_2OH) functional groups that may form in a 2, 4 or 6 position of the aromatic ring.[16] Then the -CH_2OH and hydroxyl (-OH) groups of neighboring molecules react with each other and unsubstituted resorcinol sites inducing -CH_2-O-CH_2-, -CH_2-O- and -CH_2- bridges, that connect monomers into nanometer-sized molecular clusters (oligomers), which further crosslink forming larger particles. Figure 1 summarizes this process.

Both basic or acidic catalysts have been previously used.[16] Under basic conditions, R is deprotonated, which increases electron density at the active positions of R. [18] Electron donation from those positions to the partially positively charged carbonyl carbon of F leads to the described above hydroxymethylation. The base catalyst further causes deprotonation of hydroxymethylated R, leading to a very reactive and unstable o-quinone methide intermediate [18], which react with another R molecule to form stable linkages [18]. The most common and well-studied catalyst for R-F polymerization is a sodium carbonate (Na_2CO_3), a base.[16] High concentration of this catalyst results in the formation of small (3-5 nm) interconnected polymer particles,[21] while lower concentration yield larger (up to ~ 200 nm) polymer particles, similarly interconnected and forming polymeric gels.[21, 22] In prior studies dilute weak bases, such as NH_3OH, have been used as buffers to control the pH of the initial solution.[16] They are not sufficiently active as catalysts under regular synthesis conditions.

The application of hydrothermal synthesis at elevated pressures and temperatures may accelerate polymerization significantly, even if pure NH_3OH is used in a small concentration. In contrast to prior studies, where formation of xerogels with controlled meso- and macro-pore size was of interest,[16] we were mostly interested in the formation of individual particles of controlled dimensions. Therefore, a significant degree of cross-linking within individual particles was required in order to prevent melting and fusing polymer particles together during subsequent annealing and carbonization.

Our experiments confirmed that pure NH_3OH indeed allows for the formation of uniform, individual spherical particle dispersion *via* a hydrothermal route. Similar to the currently accepted theory,[16] during the initial step of the synthesis process (30°C) the NH_3OH-catalyzed reactions link the R-F monomers (Fig. 1a) together, forming R-F polymer chains (R-F oligomesr) throughout the solution (Fig.1 b). Small weakly cross-linked R-F nanoparticles may also form. Once the

solution/suspension is then placed in a hydrothermal reactor at 100 °C, the R-F nanoparticles and oligomers cross-link together and condense to from larger particles with sufficient degree of cross-links to prevent their fusing during the subsequent heat treatments.

Table 1 shows composition of the precursor solutions used in our experiments aimed to investigate how precursor concentration would affect the morphology and size of the carbon particles.

Figure 2 shows SEM micrographs of the collected products after carbonization at 600 °C. All images show rather uniform mono-dispersed carbon spheres without impurities, such as irregularly shaped pieces of carbon. Increasing concentration of the R-F precursor in H_2O increases the average particle size quite substantially (compare RF1-RF6 samples, Fig. 2). Because all other parameters are kept constant (Table 1), the observed trends offer a simple route for the particle size control. Higher precursor concentration provides more "building material" for the growth of individual particles from oligomers. The spherical shape minimizes the surface-to-volume ratio of the polymer particles in the solution, and is typical for homogeneous nucleation of particles having no crystal structure and thus no other preferred shape that minimizes their surface energy in a solution. We also observe that particles larger than ~400 nm tend to fuse during annealing (Fig. 2e, f), suggesting that the degree of cross-linking for them was insufficient and that larger particles require hydrothermal treatment for longer time or at higher temperature.

TEM provides additional information on the homogeneity of the samples as well as on their microstructure. It further provides more details about the morphology of the smallest particles. Figure 3 shows representative TEM micrographs of the samples RF1 – RF6. The smallest particles (RF1-RF3, Fig. 3a-c) are clearly separated from each other. In contrast, the largest particles show wide necking connecting neighboring particles within small clusters (RF4-RF5, Fig. 3e, f), in accord with SEM measurements (Fig. 2 e-f). The surface of all particles is smooth and their highly disordered microstructure – very uniform within individual particles. No voids or inclusions or irregular particles could be found (Fig. 3). This is particularly clearly seen in higher resolution images of the smallest particles (RF1-RF2, Fig. 3g-h).

Diameters of approximately one hundred of random particles within each of the prepared sample were measured from TEM images by using a simple image analysis program that assumes a spherical shape of the particles. The average diameters as well as standard deviations of the diameter distributions are plotted as a function of molar ratio of H_2O to the precursor (Fig. 4a). As previously seen in SEM (Fig. 2) and TEM (Fig. 3) studies, higher molar ratio (and thus smaller R-F concentration) leads to a rapid reduction in the particle size (Fig. 4a). When we plot the average size as a function of R-F molar fraction (Fig. 4b) we observe a dependence, that could be approximated as a cubic rout. If the concentration of stable nucleas were independent of the precursor concentration, we would indeed expect to observe such a cubic rout dependence, because (i) the total volume of the produced carbon should depend liniearly on the concentration of the precursor, (ii) the total volume of carbon equals to the number of carbon particles multiplied by the volume of each particle and (iii) the radius of individual particles depends on its volume as a cubic rout. Because larger size of oligomers should be formed at higher precursor concentrations,

leading to more nuclea reaching a critical nuclea size during the nucleation period,[22] one may also expect that higher concentration should lead to higher nucleation density and thus larger total number of particles formed. In this case, the overal dependence of the average particle size would be weaker, but follow a similar general trend of leveling off at higher precursor concentrations.

Figure 4c shows the particle size distributions of the produced samples. Overall, the distibutions are rather narrow. The full width at half maximum (FWHM) of the distributions varies within 5 to 20% of the average particle size (Fig. 4d). The growth rate for various particles is expected to be similar within the synthesis reactor due to a combination of (i) good temperature uniformity within the reactor and, more importantly, (ii) continuous mixing during synthesis. Therefore, the the uniformity of the particle sizes may suggest that nucleation time was small relative to the growth time.

N_2 adsorption/desorption measurements allowed us to characterize porosity of the produced samples. Except for the three smallest particles, the shape of the isotherms is of pure Type I (in the Brunauer classification) with saturation at relative pressure (P/P_0) of ~0.1, which is characteristic for microporous materials with very low volume of pores >2 nm. Reduction of the particle size below ~ 220 nm led to the formation of the adsorption-desorption loop at the highest relative pressure values ($P/P_0 > 0.8$), which indicates additional formation of large mesopores and macropores. The adsorption-desorption hysteresis is commonly associated with capillary condensation in such mesopores.[23] Since both the surface of the particles (Fig. 2) and the bulk of the particles (Fig. 3) did not show any signs of such large pores, we assign these larger pores to the interstitial spaces between the agglomerated particles. In accord to this theory, we see that the BET (Brunauer Emmett Teller) specific surface area (SSA) of all but the smallest samples is nearly identical, as shown in Fig. 5b. This is because the internal (but open) surface area of the produced carbon samples shall be significantly larger than external area of the spheres. The BET SSA is moderate, ~600 m^2/g. If needed, subsequent activation by chemical or physical methods shall be able to increase the BET SSA to well above 2000 m^2/g.[19, 24] The non-local density functional theory (NLDFT) calculations conducted on the collected isotherms confirmed that synthesized powders are largely microporous, but those having the smallest particle size additionally showing pores > 10 nm, likely due to N_2 adsorption near a saturated pressure in the areas, where particles contact each other. Due to the ability of the N_2 sorption to measure pores of up to ~ 50 nm, the total measured pore volume gradually increases with particle size reduction (Fig. 5d) and with the corresponding increase in the volume of 10-50 nm pores formed by interstitials.

The XRD confirmed the highly disordered carbon structure observed during our TEM studies. The XRD patterns (nearly identical for all samples) exhibit two broad bands at about 22 and 44°, which we assign to diffractions on (002) and (100) planes of graphitic carbon (Fig. 6). The pattern is typical of highly disordered carbon materials, including microporous carbons.[25]

4. Summary and Conclusions

In the course of our study we have demonstrated a simple low-cost route for the formation of spherical porous carbon particles with uniform and tunable size. The application of a low

temperature (100 °C) hydrothermal reaction greatly accelerates the cross-linking within a resorcinol-formaldehyde polymer, allowing formation of individual spherical carbon particles upon subsequent polymer carbonization. XRD studies revealed highly disordered structure of the produced carbon. SEM and TEM studies showed very smooth particle surface, uniform particle density and the lack of impurities or irregularly shaped carbon particles and, for particles below ~400 nm, no particle sintering into carbon gels during carbonization. Gas sorption measurements revealed as-synthesized particles to exhibit BET SSA of ~ 600 m^2/g and this surface area is primarily built with micropore (< 2nm) walls. The large mesopores (> 10 nm) observed within the smallest particles were assigned to the inter-particle spacing. By reducing the precursor concentration we have demonstrated particle size reduction from ~1250 to 140 nm. The porous carbon particles produced with the proposed method may find a broad range of applications, from catalyst support to electrodes in energy storage devices, such as batteries and supercapacitors, to gas storage media to biological and medical sorbents.

5. References

[1] W. Gu, G. Yushin, WIREs Energy Environ 2013, doi: 10.1002/wene.102.

[2] B. Zhang, X. Qin, G. R. Li, X. P. Gao, Energy & Environmental Science 2010, 3, 1531; N. Jayaprakash, J. Shen, S. S. Moganty, A. Corona, L. A. Archer, Angewandte Chemie-International Edition 2011, 50, 5904; J. Schuster, G. He, B. Mandlmeier, T. Yim, K. T. Lee, T. Bein, L. F. Nazar, Angewandte Chemie-International Edition 2012, 51, 3591; S. B. Yang, X. L. Feng, L. J. Zhi, Q. A. Cao, J. Maier, K. Mullen, Adv. Mater. 2010, 22, 838; R. Demir Cakan, M.-M. Titirici, M. Antonietti, G. Cui, J. Maier, Y.-S. Hu, Chem. Commun. 2008, 3759; Y. H. Xu, Q. Liu, Y. J. Zhu, Y. H. Liu, A. Langrock, M. R. Zachariah, C. S. Wang, Nano Lett. 2013, 13, 470; A. Magasinski, P. Dixon, B. Hertzberg, A. Kvit, J. Ayala, G. Yushin, Nature Materials 2010, 9, 353.

[3] C. Xu, L. Cheng, P. Shen, Y. Liu, Electrochem. Commun. 2007, 9, 997.

[4] G. Yushin, R. K. Dash, Y. Gogotsi, J. Jagiello, J. E. Fischer, Adv. Funct. Mater. 2006, 16, 2288; J.-Y. Miao, D. W. Hwang, K. V. Narasimhulu, P.-I. Lin, Y.-T. Chen, S.-H. Lin, L.-P. Hwang, Carbon 2004, 42, 813; M. Sevilla, A. B. Fuertes, R. Mokaya, Energy & Environmental Science 2011, 4, 1400.

[5] S. Liu, J. Sun, Z. Huang, J. Hazard. Mater. 2010, 173, 377.

[6] A. V. Baryshev, A. B. Khanikaev, M. Inoue, P. B. Lim, A. V. Sel'kin, G. Yushin, M. F. Limonov, Phys. Rev. Lett. 2007, 99; A. A. Zakhidov, R. H. Baughman, Z. Iqbal, C. X. Cui, I. Khayrullin, S. O. Dantas, I. Marti, V. G. Ralchenko, Science 1998, 282, 897.

[7] J. E. St Dennis, K. Jin, V. T. John, N. S. Pesika, Acs Applied Materials & Interfaces 2011, 3, 2215.

[8] S. Yachamaneni, G. Yushin, S. H. Yeon, Y. Gogotsi, C. Howell, S. Sandeman, G. Phillips, S. Mikhalovsky, Biomaterials 2010, 31, 4789.

[9] Y. Wang, F. Su, J. Y. Lee, X. S. Zhao, Chemistry of Materials 2006, 18, 1347; X. Wang, P. Liu, Y. Tian, Microporous Mesoporous Mater. 2011, 142, 334.

[10] U. Jeong, Y. Wang, M. Ibisate, Y. Xia, Advanced Functional Materials 2005, 15, 1907.

[11] A. Stein, Microporous Mesoporous Mater. 2001, 44, 227.

[12] J. Lee, S. Han, T. Hyeon, Journal of Materials Chemistry 2004, 14, 478.

[13] Y. Meng, D. Gu, F. Zhang, Y. Shi, L. Cheng, D. Feng, Z. Wu, Z. Chen, Y. Wan, A. Stein, Chemistry of materials 2006, 18, 4447.

[14] P. Santhosh, K. M. Manesh, S. Uthayakumar, A. I. Gopalan, K. P. Lee, Biosensors & Bioelectronics 2009, 24, 2008.

[15] J. Liu, S. Z. Qiao, H. Liu, J. Chen, A. Orpe, D. Zhao, G. Q. Lu, Angewandte Chemie International Edition 2011, 50, 5947.

[16] S. A. Al-Muhtaseb, J. A. Ritter, Adv. Mater. 2003, 15, 101.

[17] Aegerter, M. A., Leventis, N., & Koebel, M. M. (2011). *Aerogels handbook*. New York: Springer.

[18] C. Portet, G. Yushin, Y. Gogotsi, J. Electrochem. Soc 2008, 155 (7), A531.

[19] M.-M. Titirici, M. Antonietti, Chemical Society Reviews 2010, 39, 103; B. Hu, K. Wang, L. H. Wu, S. H. Yu, M. Antonietti, M. M. Titirici, Adv. Mater. 2010, 22, 813.

[20] L. Wei, G. Yushin, Nano Energy 2012, 1, 552; L. Wei, M. Sevilla, A. B. Fuertesc, R. Mokaya, G. Yushin, Advanced Energy Materials 2011, 1, 356.

[21] X. Lu, R. Caps, J. Fricke, C. T. Alviso, R. W. Pekala, J. Non-Cryst. Solids 1995, 188, 226.

[22] R. Petricevic, M. Glora, J. Fricke, Carbon 2001, 39, 857.

[23] J. P. Schaffer, A. Saxena, S. D. Antolovich, T. H. Sanders, S. B. Warner, *The Science and Design of Engineering Materials*, McGraw-Hill, 1999.

[24] M. Rose, Y. Korenblit, E. Kockrick, L. Borchardt, M. Oschatz, S. Kaskel, G. Yushin, in *Small*, Vol. 7, 2011, 1108; W. J. Thomas, B. Crittendedn, *Adsorption technology and design*, Butterworth-Heinemann, Oxford; Boston 1998.

[25] L. Wei, N. Nitta, G. Yushin, Acs Nano 2013, 7, 6498; L. Wei, M. Sevilla, A. B. Fuertes, R. Mokaya, G. Yushin, Adv. Funct. Mater. 2011; L. Wei, G. Yushin, Power Sources 2011, 196 4072

[26] G. Laudisio, R. K. Dash, J. P. Singer, G. Yushin, Y. Gogotsi, J. E. Fischer, Langmuir 2006, 22, 8945; E. N. Hoffman, G. Yushin, T. El-Raghy, Y. Gogotsi, M. W. Barsoum, Microporous Mesoporous Mater. 2008, 112, 526; G. Yushin, E. Hoffman, A. Nikitin, H. Ye, M. W. Barsoum, Y. Gogotsi, Carbon 2005 44, 2075; E. Hoffman, G. N. Yushin, B. M. Barsoum, G. Gogotsi, Chem. Mater. 2005, 17, 2317.

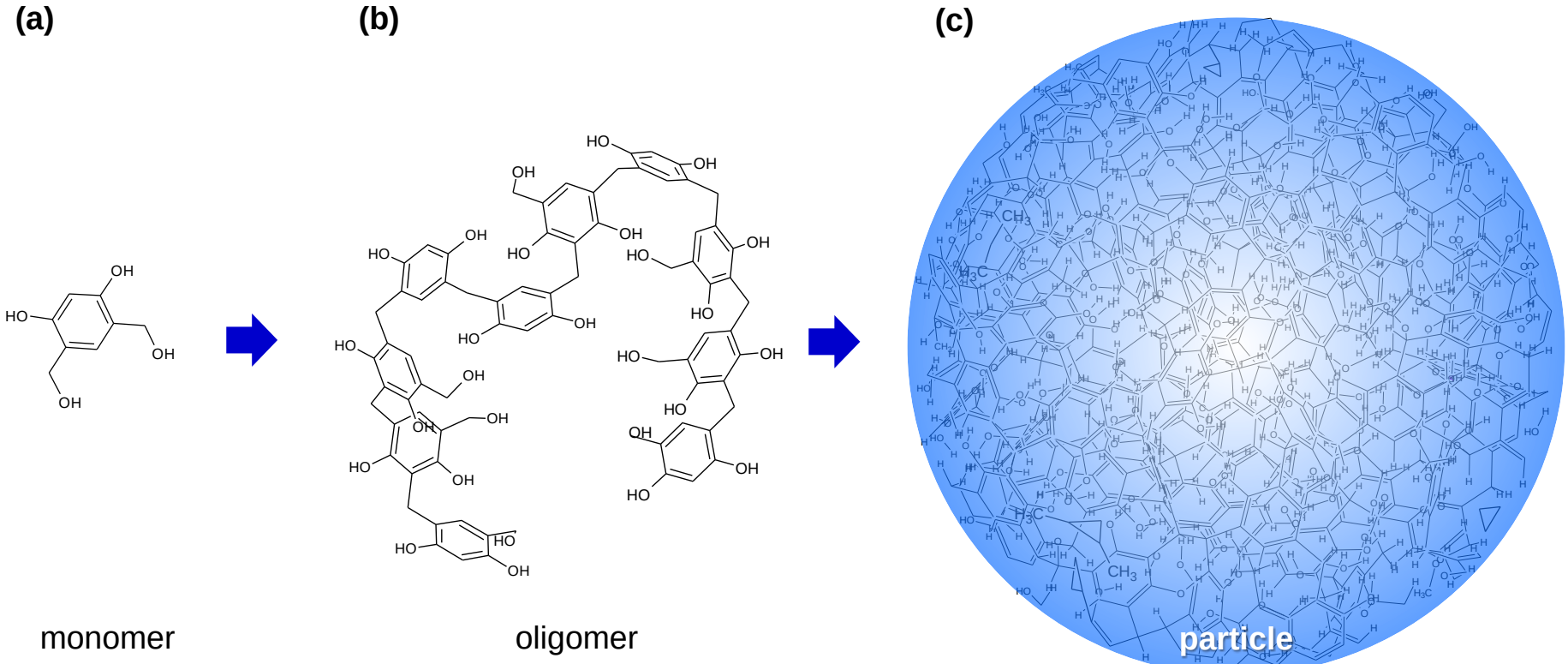

Figure 1. Simplified schematic of the formation of the R-F polymer particles

Table 1. Synthesis conditions.

Sample	H_2O (ml)	NH_4OH (ml)	Resorcinol (R) (g)	Formaldehyde (F) (37% wt.) (g)	H_2O/ (R+F) molar ratio (mol/mol)	Average diameter of carbonized particles (nm)
RF1	50	0.2	0.0887	0.125	1118	140
RF2	50	0.2	0.1337	0.200	746	220
RF3	50	0.2	0.1789	0.250	558	210
RF4	50	0.2	0.3551	0.500	281	433
RF5	50	0.2	0.7135	1.000	141	1000
RF6	50	0.2	1.4330	2.000	71	1250

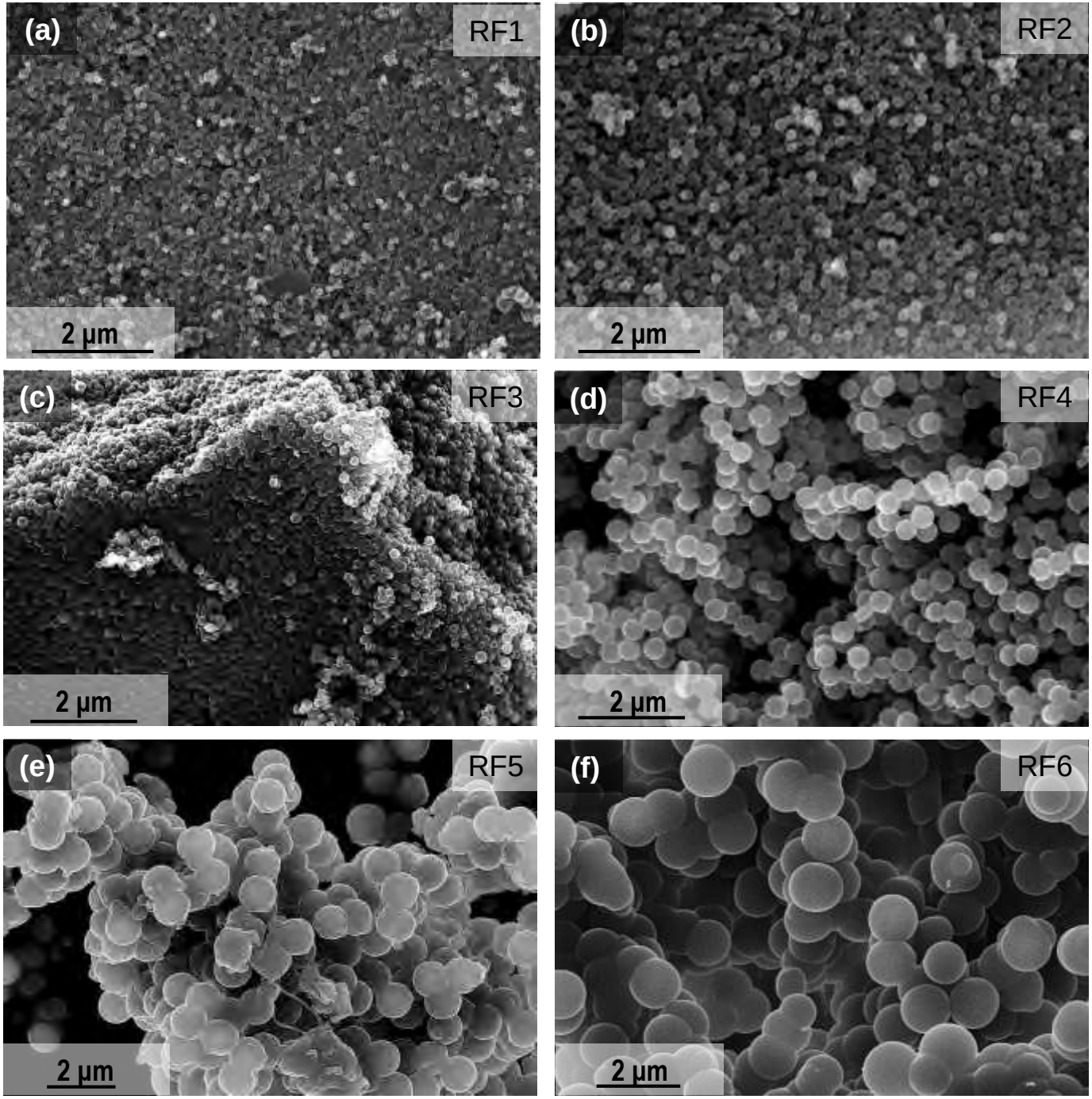

Figure 2. SEM micrographs of the spherical carbon particles synthesized under gradually reducing molar ratio of H_2O to resorcinol (R) and formaldehyde (F): (a-f) RF1-RF6.

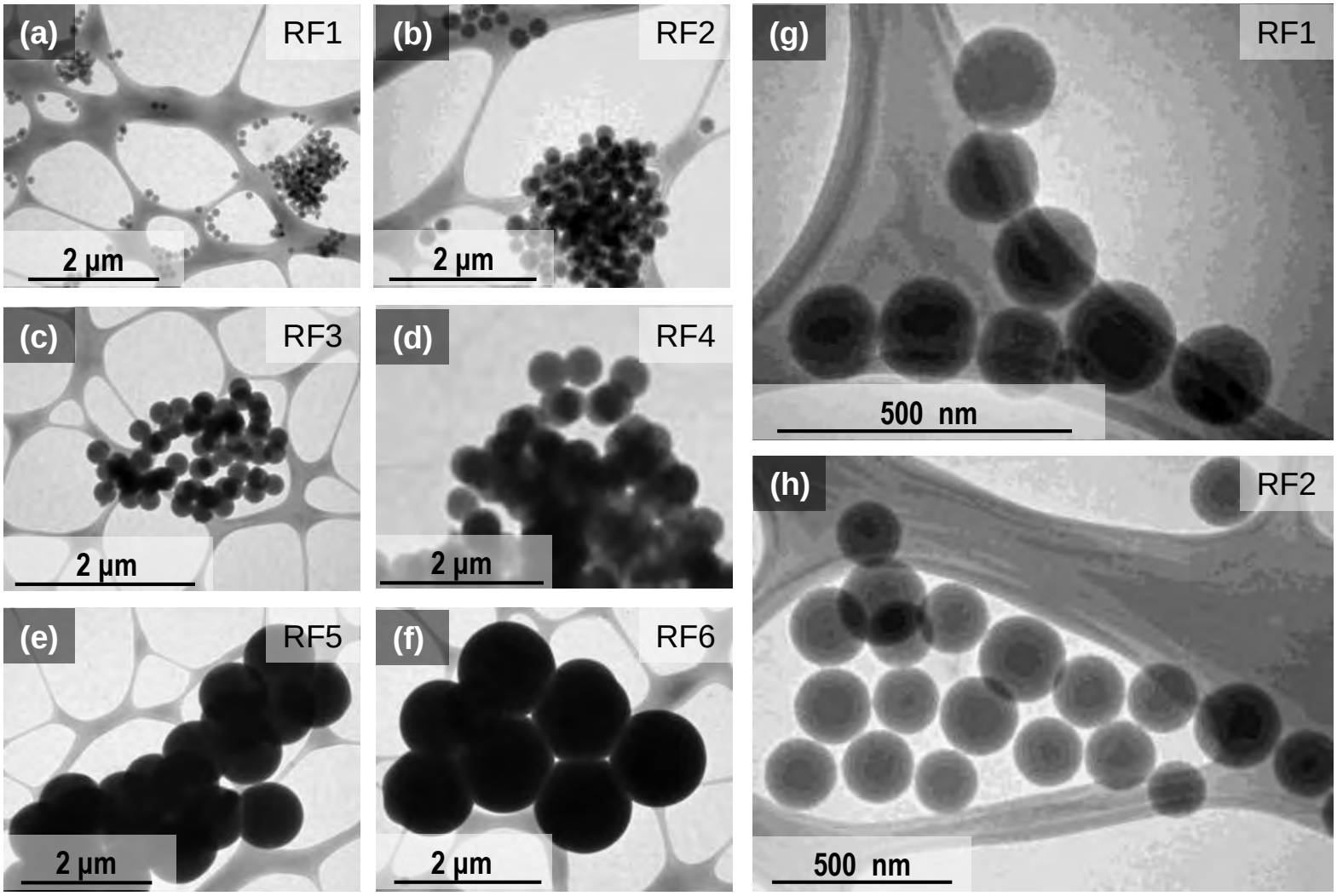

Figure 3. TEM micrographs of the spherical carbon particles synthesized under gradually reducing molar ratio of H_2O to R and F: (a-f) RF1-RF6; (g) higher magnification micrographs for RF1 and (h) RF2.

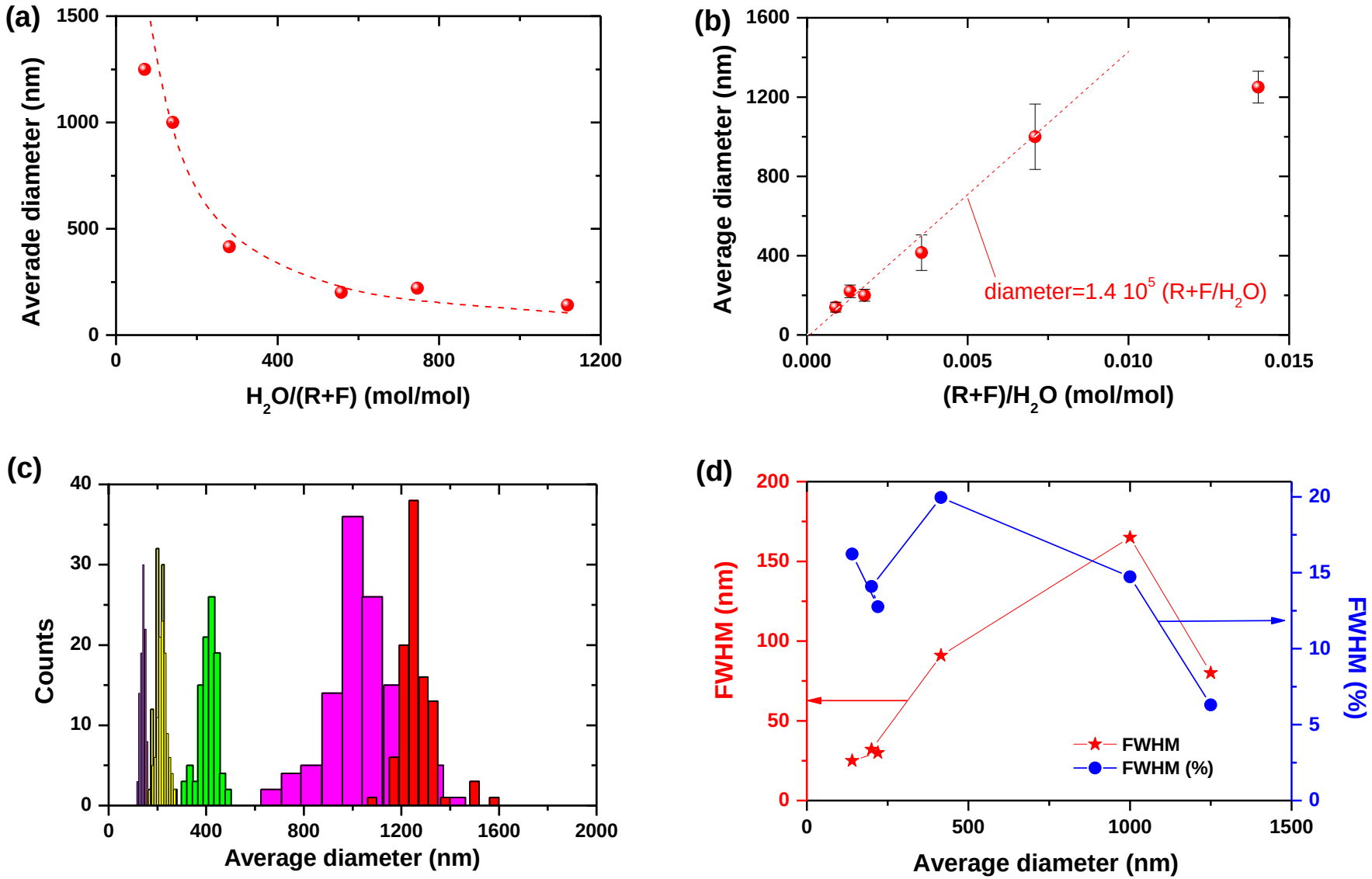

Figure 4. Synthesized particle size and size distribution: (a) average particle diameter as a function of the molar ratio of H_2O to R and F; (b) average particle diameter as a function of the molar ratio of R and F to H_2O; (c) particle size distribution; (d) full width at half maximum of the particle size distribution as a function of particle size.

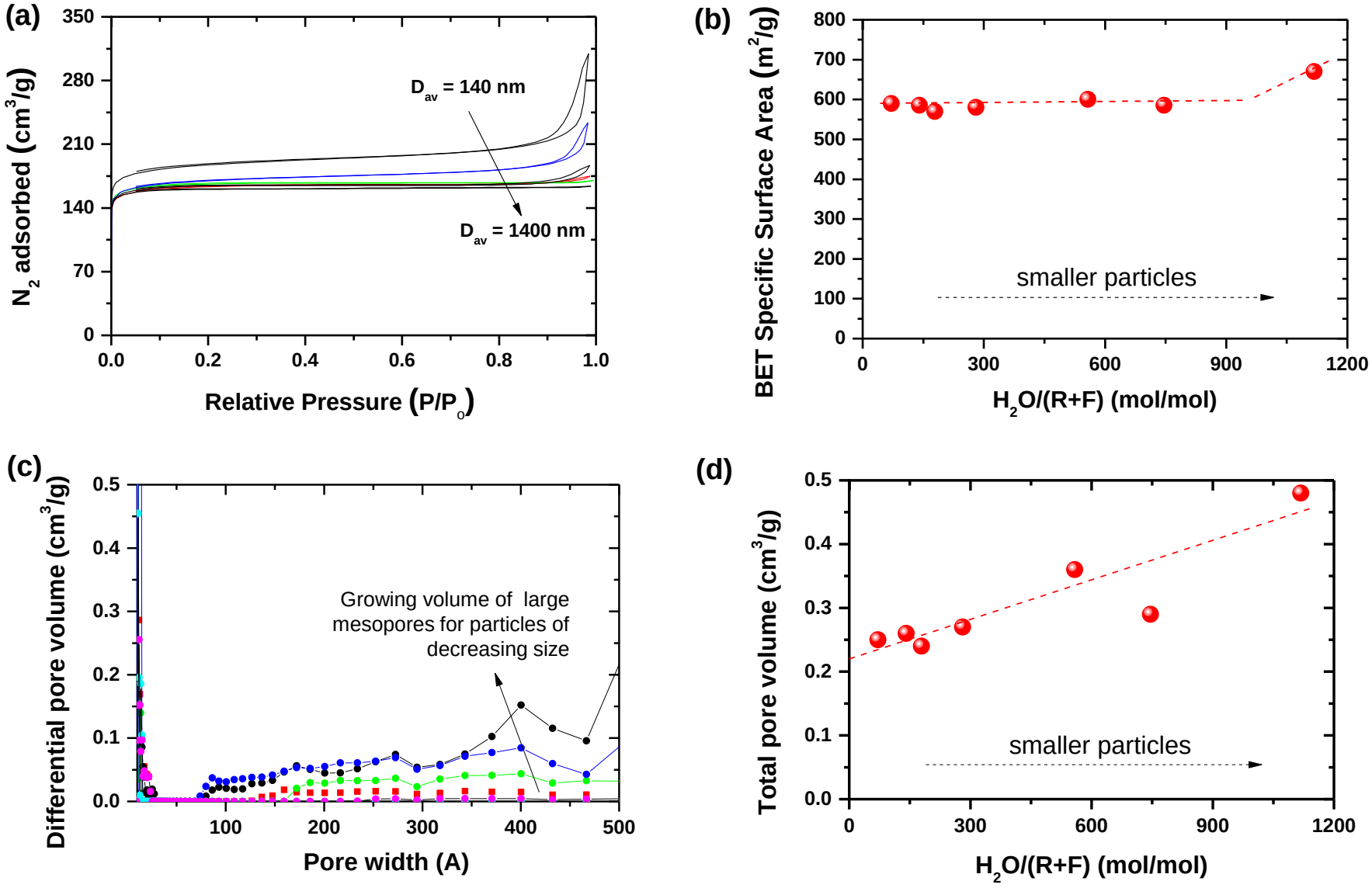

Figure 5. Porosity characterizations of synthesized particles: (a) N_2 adsorption/desorption isotherms for RF1-RF6 particles; (b) specific surface area as a function of the molar ratio of H_2O to R and F; (c) differential pore size distributions; (d) total pore volume measured from the N_2 sorption experiment as a function of the molar ratio of H_2O to R and F

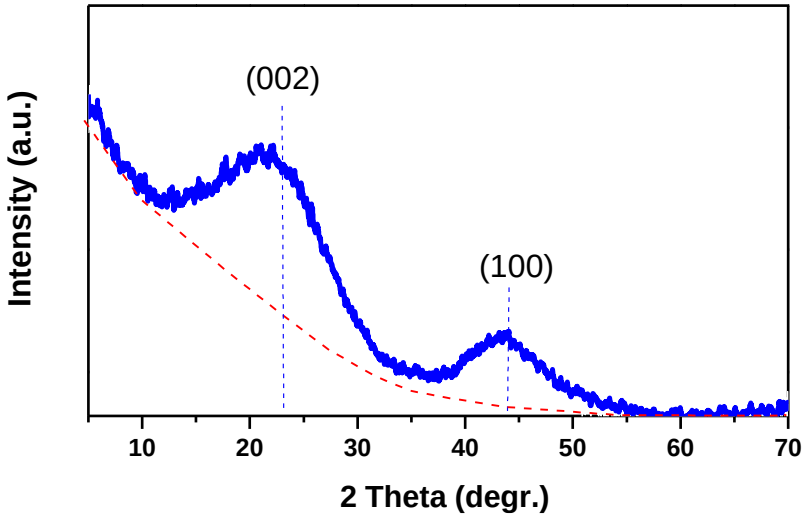

Figure 6. X-ray diffraction pattern of synthesized particles.